Use of the Connectivity Modeling System to estimate movements of red snapper (*Lutjanus campechanus*) recruits in the northern Gulf of Mexico

M. Karnauskas, J. F. Walter III, and C. B. Paris

SEDAR31-AW10

11 January 2013
Updated: 29 April 2013

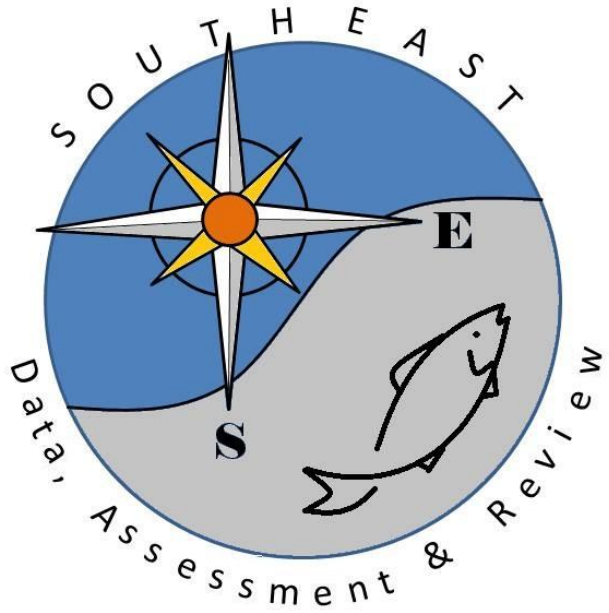

Please cite as:

Karnauskas, M., J.F. Walter, and C.B. Paris. 2013. Use of the Connectivity Modeling System to estimate movements of red snapper (*Lutjanus campechanus*) recruits in the northern Gulf of Mexico. SEDAR31-AW10. SEDAR, North Charleston, SC. 20 pp.

SEDAR31-AW10

Use of the Connectivity Modeling System to estimate movements of red snapper (*Lutjanus campechanus*) recruits in the northern Gulf of Mexico

M. Karnauskas[1], J. F. Walter III[1], and C. B. Paris[2]

[1]Southeast Fisheries Science Center

Sustainable Fisheries Division

75 Virginia Beach Drive

Miami, FL 33149-1099

[2]University of Miami

Rosenstiel School of Marine and Atmospheric Science

Department of Applied Marine Physics

4600 Rickenbacker Causeway

Miami, FL 33149

****

Panama City, FL

Introduction

The 2012 red snapper (*Lutjanus campechanus*) assessment will use a two-area Stock Synthesis model to estimate reference points for an overall northern Gulf of Mexico (GoM) stock. When parameterized for multiple areas, Stock Synthesis can account for movement of both recruits and adults between regions. Currently, there are no estimates of the extent of movement of red snapper recruits between the northeastern and northwestern GoM. The purpose of this research is to obtain estimates of the extent to which recruits move between the two areas, on an annual basis, for direct input into the red snapper Stock Synthesis model. This modeling effort also produces an index of annual recruitment deviations expected from oceanographic factors, which can be used to inform recruitment patterns in the stock assessment model. We use the Connectivity Modeling System (Paris et al. 2013), an individual-based model which estimates the movement of particles in a 3-D velocity field, and has the capacity to simulate complex behaviors such as those displayed by fish larvae. The connectivity model is used to simulate the release of red snapper eggs during the spawning season for years 2003 – 2012.

This study builds on similar work done by Johnson et al. (2012), where a numerical circulation model was used to estimate larval connectivity between Campeche Bank and the northern GoM. For the four years investigated, they found evidence of little connectivity between the two regions, and suggested that the Campeche region does not contribute significantly to the northern population. Here we focus exclusively on the northern Gulf of Mexico to investigate the nature of connectivity between the northeast and northwest, as well as expected deviations in recruitment over time, and provide specific inputs for the current red snapper Stock Synthesis assessment model.

Methods

Connectivity Modeling System

The Connectivity Modeling System (CMS) is a biophysical modeling system based on a Lagrangian framework, and was developed to study complex larval migrations (Paris et al. 2013). The CMS uses outputs from hydrodynamic models and tracks the three-dimensional movements of advected particles through time, given a specified set of release points and particle behaviors. Optional modules are provided to allow for complex behaviors and movements, simulating observed biological phenomena such as egg buoyancy, ontogenetic vertical migration, and tidal stream transport. The specific model set up used for this study is outlined in detail below.

Ocean velocity fields

The hydrodynamic model we used was the HYCOM + NCODA Gulf of Mexico 1/25° Analysis, a freely available ocean model with daily velocity fields available from 2003 – 2012 (www.hycom.org). HYCOM is a hybrid isopycnal coordinate ocean model (i.e., isopycnal in the stratified open ocean, fixed-depth in the unstratified surface layers, and terrain-following in shallow coastal waters), while allows for optimal simulation of both coastal and open-ocean features simultaneously (Chassignet et al. 2007). The model is data-assimilative, using real-time

observations of the ocean's surface via satellite altimetry, as well as vertical profile information from CTDs, the ARGO observation program, and other sources. This allows for a three-dimensional depiction of ocean currents in real time at a relatively high resolution.

Initial conditions of the biological model

Spawning time

Spawning season for both E and W populations of red snapper in the northern GoM generally begins in May and ends in early fall. Collins et al. (2001) reported a single peak from May – July for both NE and NW populations. Rooker et al. (2004) noted a single peak occurring form late May to early June for a study off the coast of Texas. Spawning is estimated to occur approximately every 3 days (Brown-Peterson et al. 2009, Jackson et al. 2006, Woods 2003) and there is no lunar periodicity apparent in the timing of spawning (Jackson et al. 2006). For our model runs, we simulated homogeneous spawning activity throughout the peak spawning period of May 1 to August 31 every year. Releases of particles representing eggs were simulated every 3 days throughout the spawning period for all 10 years.

Spawning location

Exact spawning locations of red snapper across the entire northern GoM are unknown, with only a few scattered observations having been published (e.g., Collins et al. 2001) Unlike other lutjanids, which spawn at very specific, predictable locations and times during the lunar cycle, red snapper spawn more continuously in space and time. Presumably, the spatial distribution of spawning stock biomass over the spawning season should serve as a reasonable proxy for spawning activity. In the absence of more informative proxies for spawning, we based our egg releases on a probabilistic model of red snapper biomass across space.

To determine the spatial distribution of SSB, we used the 2011 Expanded Annual Stock Assessment survey, which provides a synoptic view of the distribution of red snapper across the northern GoM during their spawning season. The survey covered the entire shelf from TX to FL, and a total of 2487 red snapper were caught in the 1171 longline stations and 1939 vertical line stations (Fitzhugh et al. 2012). Cruises were carried out from April to November and during various hours of the day. We wished to make use of the combined vertical line and longline data set to get the highest spatial resolution possible, but the two gears displayed very different size-selectivities with regards to red snapper caught. Additionally, the site selection method was changed partway through the vertical sampling survey (first the vertical lines were deployed in a paired fashion with the longlines, and later independently from the longlines around areas of known red snapper habitat), so we further classified the vertical line into two separate gear types: paired and independent. The ratio of males to females in the survey did not differ significantly by latitude, so we modeled the abundance of the entire population with the assumption that the abundance of females was proportional to total abundance.

Modeling of red snapper egg numbers across space was accomplished with a series of steps: 1) modeling the expected abundance of different age classes by depth, longitude, gear, and other sampling factors, 2) converting expected abundance to eggs via a fecundity-at-age relationship,

3) kriging the residual abundance of eggs (observed – predicted) across the domain, and 4) adding the kriging predictions to the expected number of eggs at each latitude and depth bin to create a final map of egg numbers across space. These steps are detailed in the paragraphs below.

To account for the effects of these gear selectivities in our estimates of biomass, we first created a two-stage generalized linear model to estimate the effects of gear and other sampling artifacts. Presence/absence (p) of 4 age classes were modeled as a function of age, gear type, month and hour of sampling, and the longitude and depth at which sampling was carried out:

(Eqn. 1) $logit\,(p) = \beta0 + \beta1(gear) + \beta2(age) + \beta3(gear*age) + \beta4(month) + \beta5(longitude) + \beta6(depth) + \beta7(hour)$

Abundance when present was modeled as a truncated negative binomial using the link function:

(Eqn. 2) $log\,(\mu) = \beta0 + \beta1(gear) + \beta2(age) + \beta3(gear*age) + \beta4(month) + \beta5(longitude) + \beta6(depth) + \beta7(hour)$

All variables were treated as categorical factors; longitudes were binned at 1-degree resolution, depth by 10-m bins, and time by 6-hour bins. Interaction effects between gear and age were modeled because catchability rates for both gears appeared to be largely dependent on the size of the fish. Based on the logistic model, we calculated an ROC curve, which expresses the true positive rate (sensitivity) as a function of the false positive rate (100-specificity) for each value of p. A threshold value can be specified where the sum of the sensitivity and the specificity are at their maximum. This allows us to convert the expressed probabilities of the model to presences (above the threshold) and absences (below the threshold), and thus define where red snapper are not likely to occur.

Using the parameters estimated by the generalized linear model, we predicted relative abundance of each age class across space. Predictions were made at the locations of the original data points by predicting on the depth, longitude, sampling month, hour, and gear type at that point for each age class. Both predicted and observed abundances at each data point were converted to numbers of eggs through the following calculations:

(Eqn. 3) $$E_{a,i} = \begin{cases} N_{a,i} * p_{a,i} * E_a & if\ p_{a,i} > ROC_{threshold} \\ 0 & if\ p_{a,i} < ROC_{threshold} \end{cases}$$

(Eqn. 4) $$E_i = \sum_{a=1}^{4} E_{a,i}$$

where E is the number of eggs at each data point i, a is an age class, N is the estimated abundance when present of each age class a at each data point i, p is the probability of occurrence of each age class a at each data point i, and E_a is the estimated fecundity at age. The estimated fecundity at each age class was calculated from fecundity relationships reported in Porch et al. (2013). The observed number of eggs was also calculated for each data point:

(Eqn. 5) $$E_{obs\,i} = \sum_{a=1}^{4} N_{obs\,a,i} * E_a$$

where N_{obs} is the observed abundance at age a at data point i. The residual eggs, i.e., $E_i - E_{obs\,i}$, represents variations the egg numbers not explained by our model, which are presumably due to variations in abundance due to fine-scale differences in habitat types.

This small-scale residual variation in egg numbers was interpolated across the domain through the use of kriging. Empirical variograms were created for data pairs with distances < 50 km, using the classical method of moments estimator. The variogram model was fit using ordinary least squares and with no fixed nugget. A regular grid of points (10 km resolution) was overlaid on the sampling domain, and parameters from the variogram model were used to make predictions of residual egg numbers across this grid.

To estimate the total egg numbers across the 10 km resolution grid, we extracted the latitude and depth bins in which each of the grid points fell. Using the parameter estimates from the logistic model (Eqn. 1) and truncated negative binomial model (Eqn. 2) built previously, we then calculated the expected probability of occurrence and abundance when present, at age, based on latitude and depth, but for a single standardized gear, month, and time of day. Multiplying the probability of occurrence by the abundance when present then gives us the expected abundance across the domain, in the absence of sampling artifacts. Because the logistic component of the two-stage model will not estimate a value of zero, this prediction gives a non-zero abundance value for each grid point and each age. To determine where across the domain red snapper are not likely to occur, we used kriging to interpolate the logistic probability of occurrence component of the model across the domain. Again, we used the classical method of moments estimator for data pairs with distances <50 km, and fit the variogram model using ordinary least squares with no fixed nugget. Expected number of eggs at each grid cell, based on latitude and depth bin, was then calculated using Eqns. 3 and 4.

Total egg number at each grid cell was calculated by adding the expected eggs (based on the depth and longitude) to the residual eggs (based on the kriging predictions). Particle releases were carried out in CMS at each grid cell where $E > 0$ by releasing E eggs at each release time step (i.e., every 3 days throughout the spawning season). Numbers of eggs released from each grid cell were kept constant throughout all years, as our goal was to understand differences in recruitment from year to year unrelated to the level of SSB.

Settlement

Red snapper begin settling out of the pelagic stage no earlier than 26 days, with most settling by 28 days of age, and maximum settlement age is estimated to be about 30 d (Szedlmayer and Conti 1999, Drass et al. 2000, Rooker et al. 2004). We therefore specified the settlement competency period as lasting for 5 days (26-30 d). High-value settlement habitat is estimated to occur between 15 and 64 m depth (Johnson et al. 2012). We downloaded the global 30 arc-second bathymetry data grid available from GEBCO (General Bathymetric Chart of the Oceans; www.gebco.net), and extracted contours at the 15 and 64 m isobaths for the northern GoM. Suitable settlement habitat was defined by the area between these isobaths (Fig. 1). The settlement habitat was divided into 102 roughly equally-sized polygons, so that simulated particles could be tracked from source to sink. Successful settlement is defined by those particles which reach the suitable settlement habitat during the competency window.

Vertical movement

In the CMS, vertical movements are defined via a probability matrix, which specifies the distribution of particles in the water column throughout time. Time steps for the probability matrix are most logically defined by using different stages of larval metamorphosis (e.g., preflexion, postflexion), as lutjanids tend to shift in their vertical distributions with these changes. Red snapper eggs are known to hatch at approximately 24 hours after fertilization (Rooker et al. 2004). Based on a study of reared larvae, Drass et al. (2000) showed that notochord flexion began at 12 days after hatching and was complete by 15 days after hatching. We therefore defined the following phases (in days after release): hatching 0-1 days, preflexion 2-12 days, flexion 13-16 days, postflexion 17-25 days.

Little is known on the vertical movements of the red snapper in its pelagic larval stage. For example, a detailed study of lutjanid movements by phase in the FL straits reported capture of only two individual red snappers, which were insufficient to describe the pelagic larval dynamics for the species (D'Alessandro et al. 2010). Johnson et al. (2012) reported unpublished data (G. Zapfe) which showed that red snapper larvae were most numerous within the upper 30 m of the water column, suggesting vertical distributions similar to other lutjanid species. Based on the depth of initial spawning, average PLD, and average lengths of adult, we presumed that *L. analis* might be the congener most closely approximating larval movements, and we used the vertical migration information from this species as our best estimate of the movements of red snapper larvae. However, because this was the greatest area of uncertainty regarding the reproductive and larval biology of the red snapper, and because larval transport patterns are very sensitive to changes in the depth at which larvae occur, we carried out a series of sensitivity runs to quantify the effect of this uncertainty on our estimates. We altered the vertical distributions of the larvae by 1) increasing the standard deviations of the distributions and 2) moving the mean of the distributions slightly shallower and deeper in the water column (Fig. 2). For each vertical distribution, the CMS was rerun using the same assumptions with regards to other biological attributes, and the recruitment indices recalculated.

Other CMS specifications

We used the built-in turbulence module of the CMS, which adds a random component to the motion of the particles to represent turbulent diffusion. This component represents sub-grid turbulent processes not resolved by the resolution of the hydrodynamic model. We used a value of 10 $m^2 s^{-1}$ for horizontal diffusivity and 1 $m^2 s^{-1}$ for vertical diffusivity. We also used the 'avoid coast' algorithm built in the CMS, which helps to prevent particles from getting stranded on the land mask. Because fish larvae are not passive drifters, they can likely swim away from the coast to avoid being stranded. This module thus provides a more realistic estimate of the movements of fish larvae near coasts.

Results

Model of predicted fecundity index over the study domain

The selected model, based on the lowest AIC value, included all factors: gear, age class, month and hour of sampling, longitude, depth, and the gear x age interaction (Tables 1 and 2). In the logistic model, gear type explained the greatest amount of deviance in the model (9.1%) followed by depth (9.0%), longitude (6.7%), the age class x gear interaction factor (2.5%), and hour and age class (<1%). Probability of red snapper presence was estimated to be highest off the coasts of Texas and Louisiana (Fig. 3). All age classes were also predicted to occur, with slightly lower probabilities, off the Florida Big Bend region. The ROC curve analysis of the logistic regression resulted in a false positive rate of 0.29, and the false negative rate was 0.13. Variogram models, constructed for both the residual numbers of eggs and the probability of occurrence by age class, showed good fits (Fig. 4). Spatial autocorrelation of these prediction points was estimated to occur up to approximately 10 km.

The final estimated index of fecundity was highest off the coast of Texas, with a smaller area of relatively high fecundity off the Big Bend region (Fig. 5). Generally, for the northwestern GoM, nearly all grid cells were estimated to have some level of spawning biomass, whereas biomass was limited to a smaller depth range in the northeast GoM. South of the Tampa Bay region, red snapper were not predicted to occur, except for a few small isolated patches.

Connectivity modeling

The results presented here are based on simulations where the total number of particles released was kept constant across months and across years. This allows us to consider changes in recruitment patterns due exclusively to annual variation in ocean current patterns, and not related to SSB. In interpreting the results, it is also important to note that we first considered the movement of particles in the northern GoM and therefore recruitment from other locations is not accounted for.

Relative recruitment success across the entire northern GoM varied across years, with the greatest number of successful recruits occurring in 2012 (Fig. 6). Other years with relatively high recruitment were 2004, 2005, and 2006. The lowest estimated recruitment level occurred in 2008. While the recruitment index varied depending on the vertical larval distribution patterns assumed, the sensitivity runs largely agreed in regards to general trends. For example, all sensitivity runs estimated that 2008 was the year of worst recruitment success, while 2012 was the year of highest predicted recruitment success.

Spatial patterns in recruitment were also variable among years (Fig. 7). The majority of particles were predicted to self-recruit to their respective regions (W to W or E to E). Recruitment from one region to another varied through time, but in general was limited, with an average of only 4% of successfully-recruited larvae released from the west moving from west to east, and 18% of successfully-recruited larvae released from the east moving west (Table 3). Recruitment was poor in the West Florida Shelf, with a small number of recruits appearing in the southern extent of the Shelf only in select years.

Discussion

These results show that red snapper larvae are likely to be largely self-recruiting, and that mixing of larvae between the E and W regions does occur but in limited amounts. Patterns in recruitment variability over years will be further considered in light of recruitment anomalies estimated from stock assessment models. Further work will be done to consider the effects of inclusion of a recruitment index in the current Stock Synthesis model. Finally, particle trajectories will be analyzed in relation to oceanic processes, to understand the mechanisms by which successful recruitment events occur in time and space.

References

Brown-Peterson, N.J., K.M. Burns and R.M. Overstreet. 2009. Regional Differences in Florida Red Snapper Reproduction. Faculty Publications from the Harold W. Manter Laboratory of Parasitology. Paper 438.

Chassignet, E.P, H.E. Hurlburt, O. M. Smedstad, G.R. Halliwell, P.J. Hogan, A.J. Wallcraft, R. Baraille and R. Bleck. 2007. The HYCOM (HYbrid Coordinate Ocean Model) data assimilative system. Journal of Marine Systems 65:60- 83

Collins, L.A., G.R. Fitzhugh, L. Mourand, L.A. Lombardi, W.T. Walling, Jr., W.A. Fable, M.R. Burnett, and R.J. Allman. 2001. Preliminary results from a continuing study of spawning and fecundity in the red snapper (Lutjanidae: *Lutjanus campechanus*) from the Gulf of Mexico, 1998-1999. Proceedings of the 52nd Annual Gulf and Caribbean Fisheries Institute 52:34-47.

D'Alessandro, E.K., S. Sponaugle and J.E. Serafy. 2010. Larval ecology of a suite of snappers (family: Lutjanidae) in the Straits of Florida, western Atlantic Ocean. Marine Ecology Progress Series 410:159-175.

Drass, D. M., K. L. Bootes, J. Lyczkowski-Shultz, B. H. Comyns, G. H. Holt, C. M. Riley, and R. P. Phelps. 2000. Larval development of red snapper Lutjanus campechanus, and comparisons with co-occurring snapper species. U.S. National Marine Fisheries Service Fishery Bulletin 98(3):507–527.

Fitzhugh, G.R., E.T. Lang, and H. Lyon. 2012. Expanded Annual Stock Assessment Survey 2011: Red Snapper Reproduction. SEDAR31-DW07. SEDAR, North Charleston, SC. 33 pp.

Johnson, D.W., H.M. Perry and J. Lyczkowski-Shultz. 2012. Connections between Campeche Bank and Red Snapper Populations in the Gulf of Mexico via modeled larval transport. SEDAR31-RD45. SEDAR, North Charleston, SC. 31 pp.

Paris C.B, J. Helgers, E. Von Sebille and A. Srinivasan. 2013. Connectivity Modeling System: a probabilistic modeling tool for the multi-scale tracking of biotic and abiotic variability in the ocean. Environ. Modelling and Software. 42:47-54.

Porch, C.E., G.R Fitzhugh and B.C. Linton. 2013. Modeling the dependence of batch fecundity and spawning frequency on size and age for use in stock assessments of red snapper in U.S. Gulf of Mexico waters. SEDAR31-AW03. SEDAR, North Charleston, SC. 22 pp.

Rooker, J. R., A. M. Landry, B. W. Geary, and J. A. Harper. 2004. Assessment of a bathymetric high and associated habitats as nursery grounds of postsettlement red snapper. Estuarine, Coastal, and Shelf Science 59:653–661.

Szedlmayer, S.T., and J. Conti. 1999. Nursery habitats, growth rates, and seasonality of age-0 red snapper, Lutjanus campechanus, in the northeast Gulf of Mexico. Fisheries Bulletin 97:626-635.

Woods, M.K. 2003. Demographic differences in reproductive biology of female red snapper (*Lutjanus campechanus*) in the northern Gulf of Mexico. Thesis. Department of Marine Sciences, University of South Alabama, Dauphin Island, Alabama. 128 pages.

Table 1. Estimated parameters from the selected generalized linear model of red snapper probability of occurrence.

	Esti	Std. Error	z value	Pr(>|z|)	
(Intercept)	-3.85	0.29	-13.50	<0.001	***
age class 5	0.36	0.21	1.67	0.094	
age class 6	0.60	0.20	2.95	0.003	**
age class 7+	1.56	0.19	8.34	<0.001	***
gear VLpaired	-1.73	0.38	-4.59	0.001	**
gear VLindependent	1.11	0.19	5.92	0.001	**
depth [30,40]	1.76	0.17	10.31	<0.001	***
depth [40,50]	1.74	0.18	9.75	<0.001	***
depth [50,60]	1.76	0.17	10.50	<0.001	***
depth [60,70]	2.22	0.17	13.00	<0.001	***
depth [70,80]	1.78	0.19	9.62	<0.001	***
depth [80,90]	2.34	0.21	11.38	<0.001	***
depth [90,100]	2.40	0.20	11.99	<0.001	***
depth [100,500]	-0.54	0.22	-2.42	0.015	*
longitude [-96,-95]	0.29	0.20	1.47	0.142	
longitude [-95,-94]	0.03	0.17	0.16	0.875	
longitude [-94,-93]	0.39	0.16	2.40	0.016	*
longitude [-93,-92]	0.10	0.18	0.54	0.591	
longitude [-92,-91]	0.07	0.19	0.38	0.701	
longitude [-91,-90]	-0.07	0.24	-0.30	0.766	
longitude [-90,-89]	0.93	0.21	4.43	0.001	**
longitude [-89,-88]	-0.19	0.20	-0.95	0.341	
longitude [-88,-87]	-0.47	0.22	-2.15	0.032	*
longitude [-87,-86]	-0.89	0.24	-3.74	0.001	**
longitude [-86,-85]	-0.19	0.18	-1.03	0.304	
longitude [-85,-84]	-1.04	0.19	-5.52	0.001	**
longitude [-84,-81]	-2.34	0.23	-10.10	<0.001	***
month 5	-0.02	0.15	-0.10	0.918	
month 6	-0.23	0.16	-1.47	0.143	
month 7	-0.55	0.20	-2.71	0.007	**
month 8	-0.61	0.14	-4.26	0.000	***
month 9	-0.23	0.17	-1.36	0.173	
month 10	-0.70	0.17	-4.06	0.000	***
hour [6,12]	0.16	0.13	1.24	0.217	
hour [12,18]	0.21	0.12	1.75	0.080	
hour [18,23]	0.38	0.13	2.95	0.003	**
age class 5:gear VLpaired	-0.77	0.57	-1.34	0.179	
age class 6:gear VLpaired	-1.43	0.64	-2.24	0.025	*
age class 7+:gear VLpaired	-2.68	0.70	-3.85	0.000	***
age class 5:gear VLindependent	-0.52	0.25	-2.13	0.033	*
age class 6:gear VLindependent	-1.11	0.24	-4.57	<0.001	***
age class 7+:gear VLindependent	-2.27	0.23	-9.82	<0.001	***

Table 2. Estimated parameters from the selected generalized linear model of red snapper abundance when present.

	Estimate	Std. Error	z value	Pr(>|z|)	
(Intercept):1	-0.61	0.45	-1.36	0.175	
(Intercept):2	-0.38	0.10	-3.93	<0.001	***
age class 5	0.70	0.37	1.91	0.057	
age class 6	0.84	0.35	2.37	0.018	*
age class 7+	1.39	0.32	4.31	<0.001	***
gear VLpaired	1.05	0.59	1.76	0.079	
gear VLindependent	1.80	0.32	5.59	<0.001	***
longitude [-96,-95]	0.05	0.26	0.20	0.843	
longitude [-95,-94]	-0.06	0.22	-0.25	0.800	
longitude [-94,-93]	0.24	0.22	1.10	0.270	
longitude [-93,-92]	-0.23	0.24	-0.94	0.348	
longitude [-92,-91]	-0.34	0.25	-1.37	0.172	
longitude [-91,-90]	-0.46	0.33	-1.38	0.167	
longitude [-90,-89]	-0.02	0.26	-0.10	0.924	
longitude [-89,-88]	-0.46	0.27	-1.73	0.084	
longitude [-88,-87]	-0.48	0.31	-1.59	0.113	
longitude [-87,-86]	-0.99	0.36	-2.77	0.006	**
longitude [-86,-85]	-0.29	0.25	-1.15	0.250	
longitude [-85,-84]	-0.68	0.27	-2.50	0.013	*
longitude [-84,-81]	-1.60	0.45	-3.55	<0.001	***
depth [30,40]	-0.04	0.25	-0.14	0.885	
depth [40,50]	-0.25	0.27	-0.94	0.350	
depth [50,60]	0.42	0.24	1.77	0.077	
depth [60,70]	0.19	0.24	0.79	0.428	
depth [70,80]	0.00	0.26	0.01	0.993	
depth [80,90]	0.54	0.27	1.95	0.051	
depth [90,100]	-0.18	0.28	-0.63	0.526	
depth [100,500]	-0.14	0.35	-0.40	0.690	
month 5	-0.45	0.20	-2.26	0.024	*
month 6	-0.62	0.21	-2.92	0.004	**
month 7	-0.14	0.28	-0.49	0.627	
month 8	-0.23	0.19	-1.22	0.221	
month 9	0.14	0.23	0.61	0.540	
month 10	-0.81	0.23	-3.52	<0.001	***
hour [6,12]	0.06	0.19	0.30	0.767	
hour [12,18]	-0.02	0.16	-0.10	0.919	
hour [18,23]	0.13	0.17	0.73	0.467	
age class 5:gear VLpaired	-0.09	0.83	-0.11	0.914	
age class 6:gear VLpaired	-0.88	0.94	-0.94	0.346	
age class 7+:gear VLpaired	-22.63	5782.40	0.00	0.997	
age class 5:gear VLindependent	-1.19	0.39	-3.02	0.003	**
age class 6:gear VLindependent	-1.96	0.39	-4.97	<0.001	***
age class 7+:gear VLindependent	-2.43	0.37	-6.60	<0.001	***

Table 3. Percentage of particles successfully recruited, by year and region.

	West		East	
Year	to West	to East	to East	to West
2003	97.35	2.65	80.05	19.95
2004	98.18	1.82	71.85	28.15
2005	99.04	0.96	66.68	33.32
2006	98.14	1.86	86.02	13.98
2007	97.99	2.01	66.94	33.06
2008	98.24	1.76	80.87	19.13
2009	92.55	7.45	86.78	13.22
2010	94.02	5.98	91.99	8.01
2011	88.62	11.38	99.68	0.32
2012	95.07	4.93	92.49	7.51
Mean	95.92	4.08	82.34	17.66

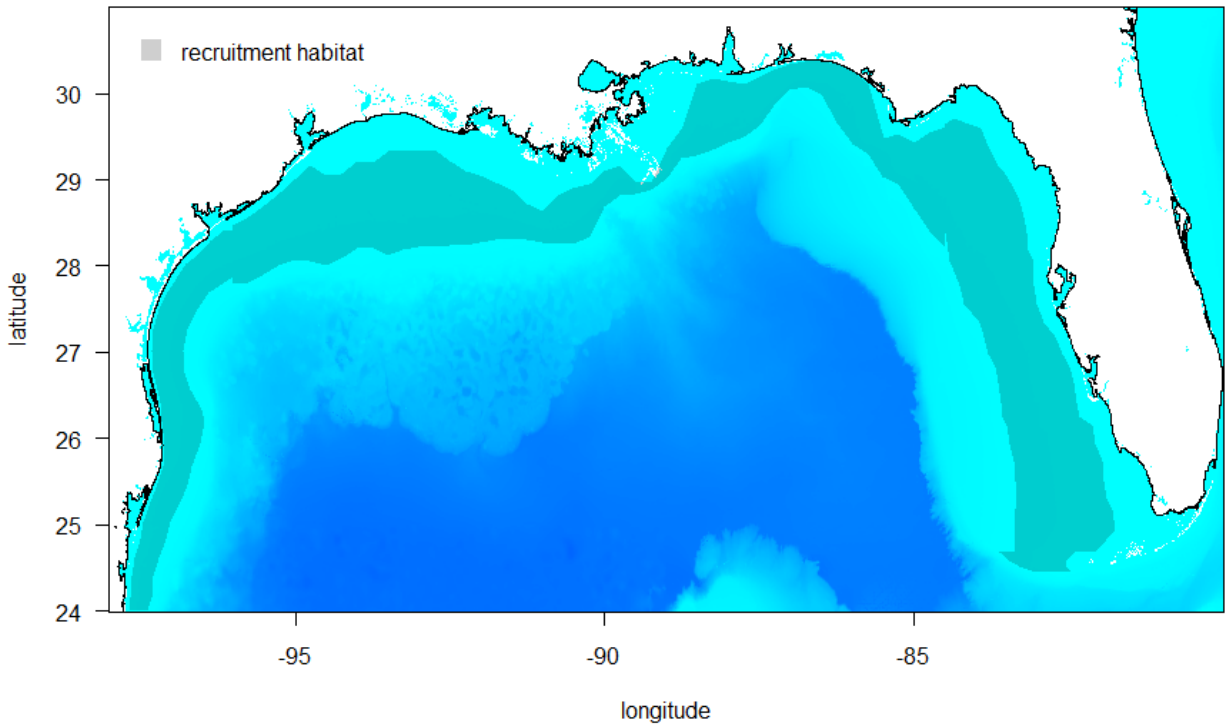

Figure 1. Map of assumed suitable recruitment habitat for red snapper. The habitat was divided into 102 polygons of approximately equal area.

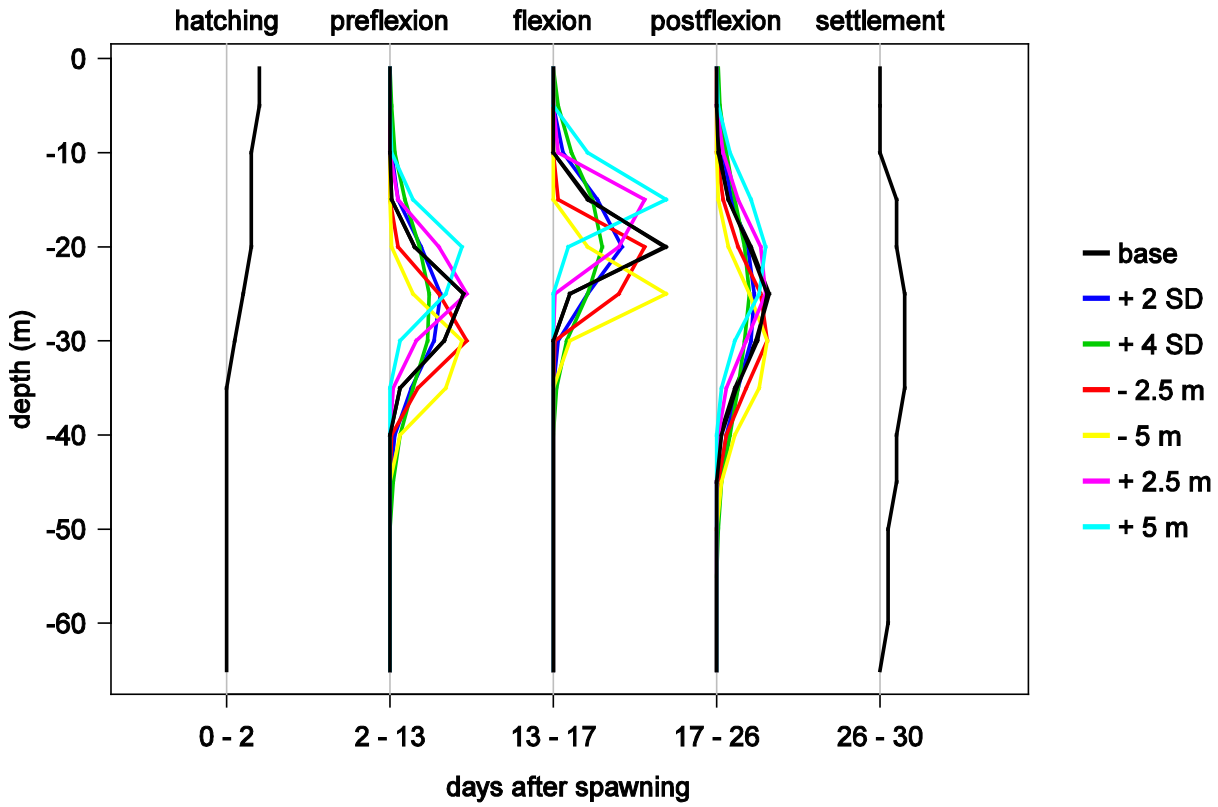

Figure 2. Visualization of the specified probability matrix defining simulated red snapper vertical larval migrations over time. Different colors denote the assumptions made for individual sensitivity runs.

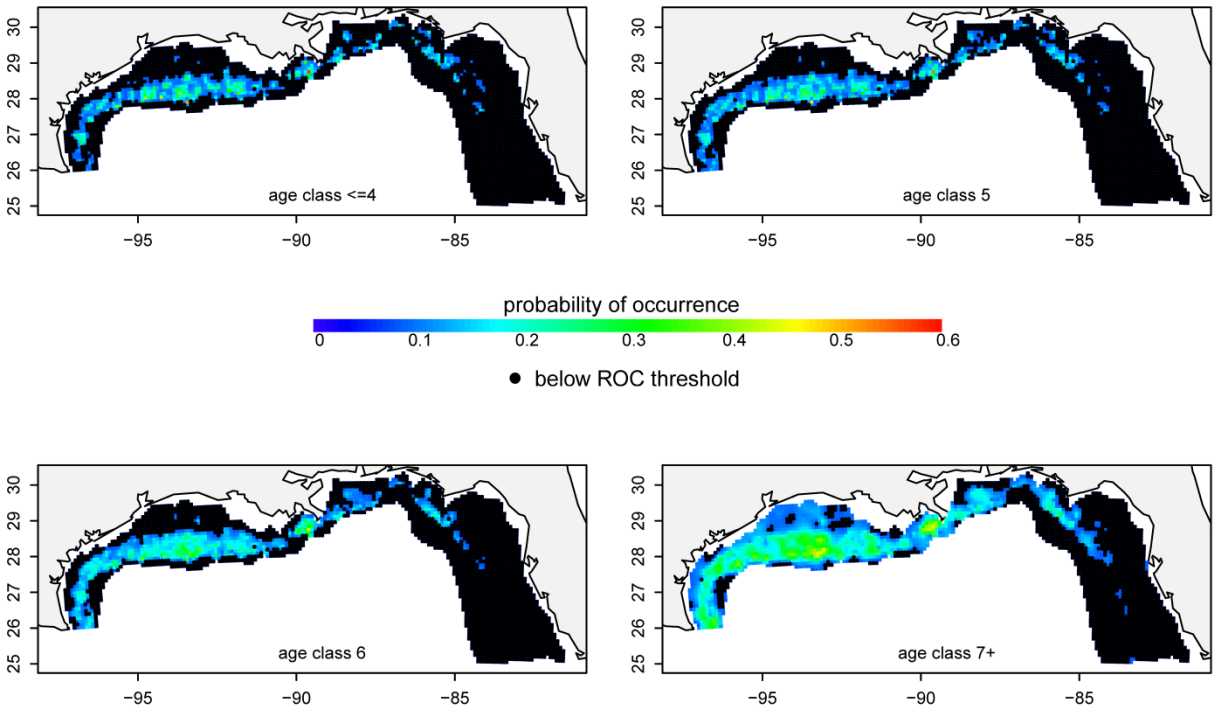

Figure 3. Kriging predictions for the probability of occurrence by age class. Grid cells with values below the ROC threshold (probable absences) are denoted with black dots.

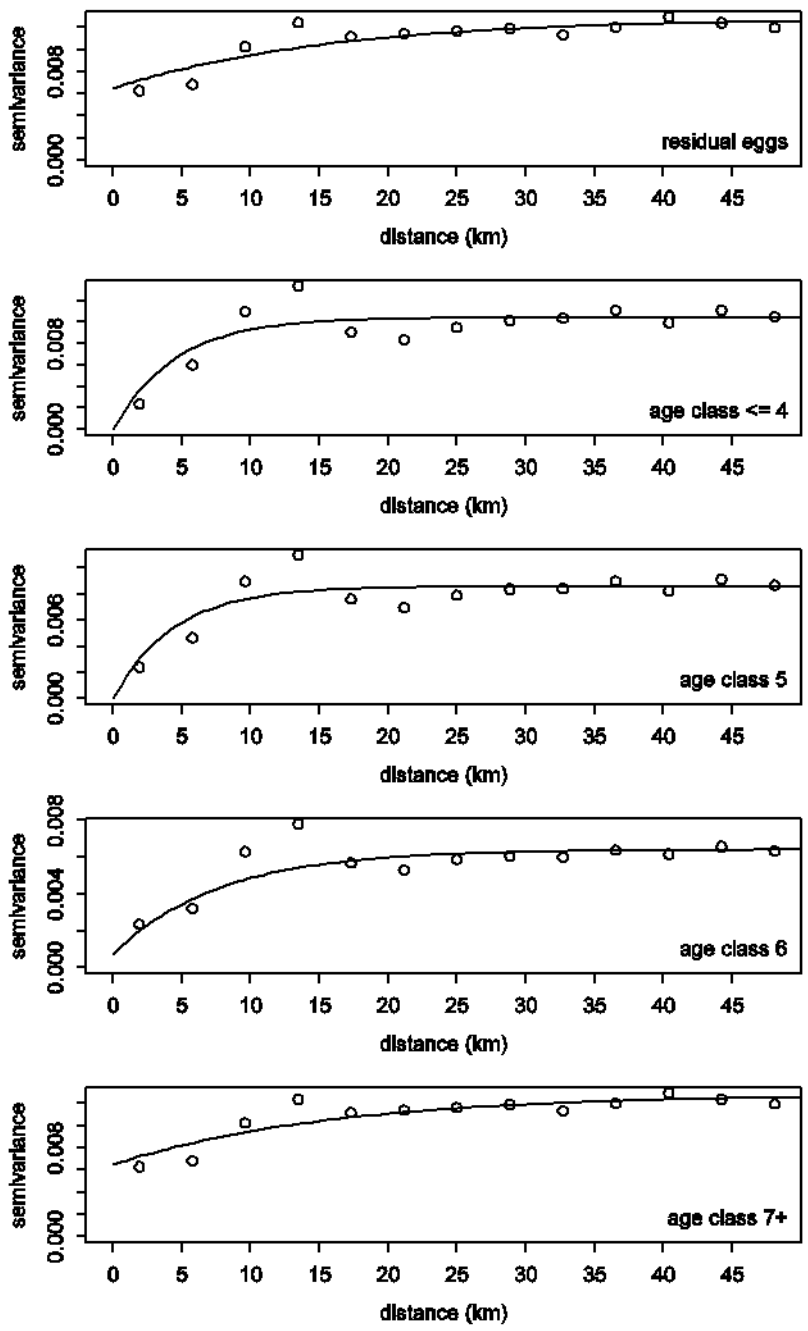

Figure 4. Variogram model fits used for kriging model residual egg nubmers and probabilities of occurrence by age.

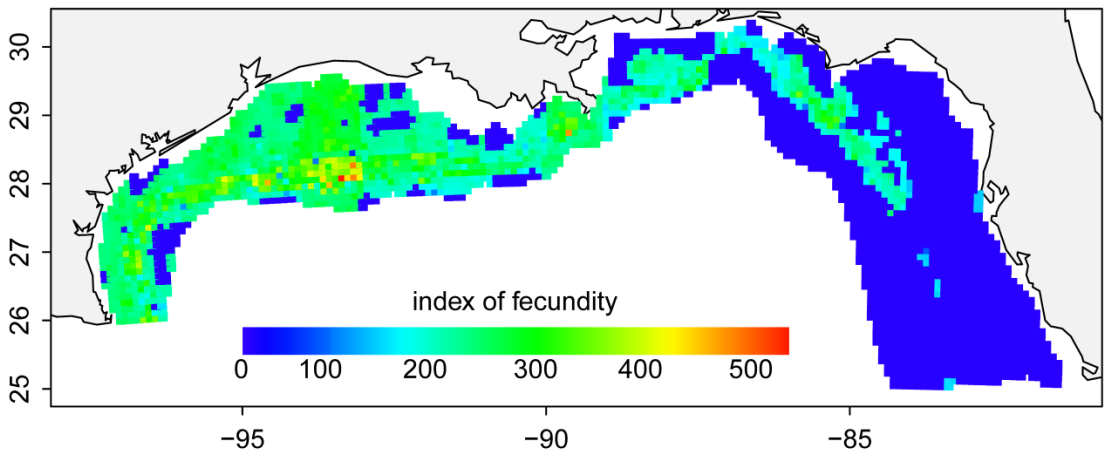

Figure 5. Final predictive map showing the index of total numbers of eggs over the 10 km resolution prediction grid. Particles were released from grid cells where the total estimated fecundity index was greater than zero. Numbers of particles released from each grid cell were scaled relative to the index.

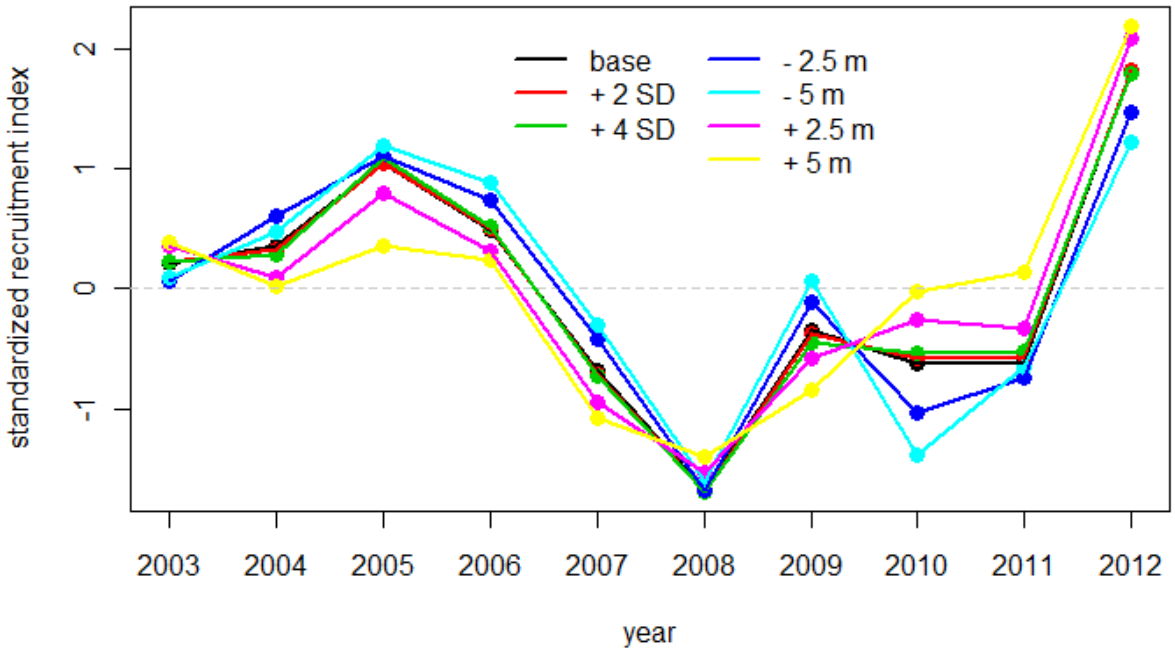

Figure 6. Index of overall recruitment success for northern GoM red snapper by year as estimated by the individual vertical distribution sensitivity runs.

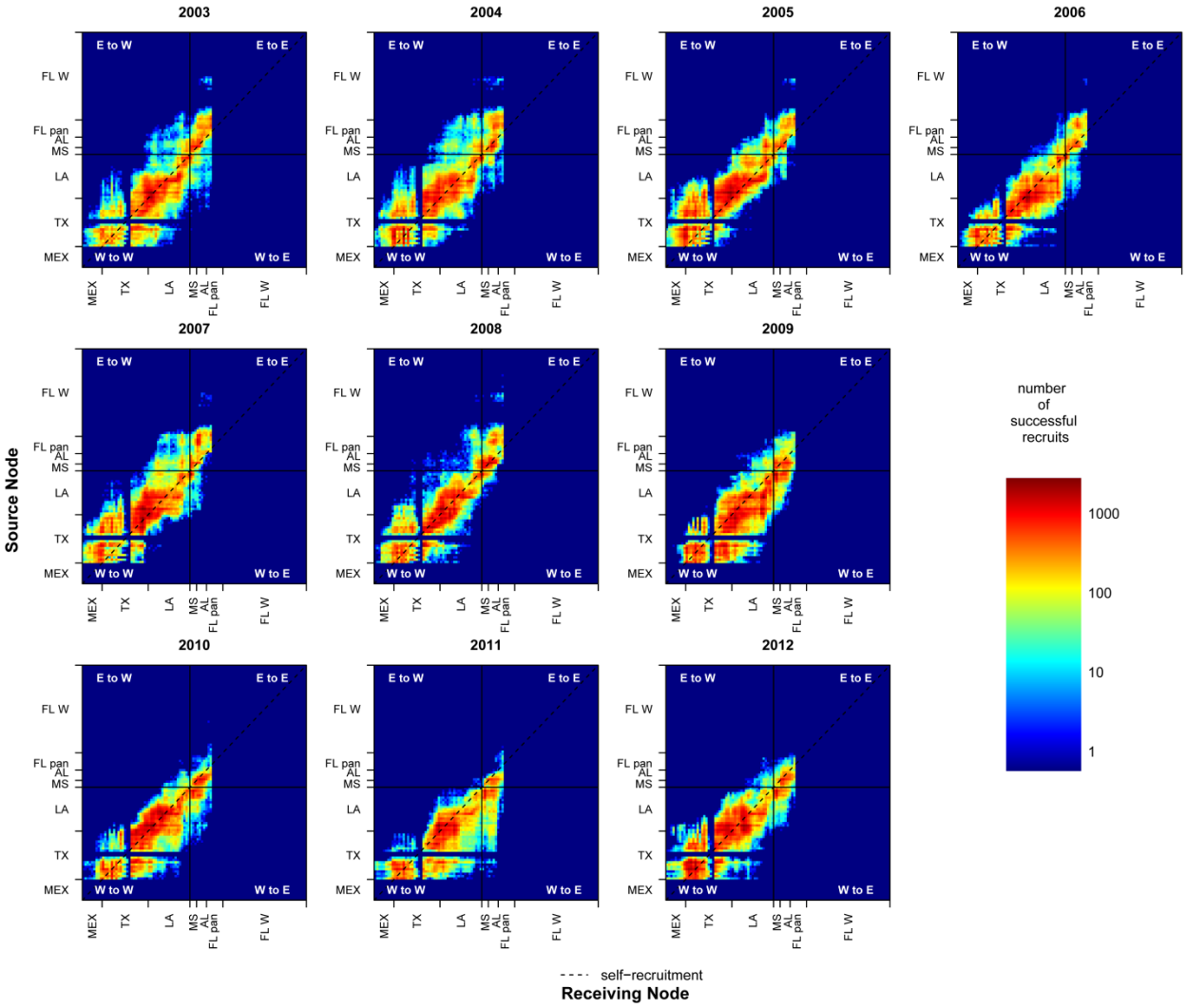

Figure 7. Connectivity matrices for the base model run showing variation in spatial recruitment patterns by year. Rows are source nodes (particle release sites) and columns are receiving nodes (particle settlement sites); nodes are ordered clockwise from Mexico to Florida. Self-recruitment is indicated by the dashed diagonal line. Solid lines denote split between west and east (the LA-MS border).